Molecular Therapy
Nucleic Acids
Original Article

Crosstalk of mRNA, miRNA, lncRNA, and circRNA and Their Regulatory Pattern in Pulmonary Fibrosis

Changye Li,[1,4] Zhenkai Wang,[2,4] Jinjin Zhang,[1,4] Xueying Zhao,[3] Pan Xu,[2] Xiangyong Liu,[1] Minge Li,[3] Changjun Lv,[1,2] and Xiaodong Song[1]

[1]Department of Cellular and Genetic Medicine, School of Pharmaceutical Sciences, Binzhou Medical University, Yantai 264003, China; [2]Department of Respiratory Medicine, Binzhou Medical University Hospital, Binzhou Medical University, Yantai 264003, China; [3]Department of Clinical Nursing, Binzhou Medical University Hospital, Binzhou Medical University, Binzhou 256602, China

Noncoding RNAs (ncRNAs), such as microRNA (miRNA), long ncRNA (lncRNA), and circular RNA (circRNA), are regulators of important biological functions. Therefore, understanding their crosstalk and regulatory patterns can provide treatment for diseases. In this study, differentially expressed RNA transcripts were obtained by RNA sequencing in bleomycin-induced pulmonary fibrosis in mice. Four miRNAs, 10 lncRNAs, and two circRNAs were tested to validate the sequencing. There were differentially expressed 585 mRNAs, 236 miRNAs, 272 lncRNAs, and 74 circRNAs in pulmonary fibrosis. Their location on chromosome, length varieties, interaction, and host genes were analyzed. lnc949, circ949, and circ057 were chosen to explore the detailed crosstalk and regulatory pattern, which were measured by using RNA-FISH, dual-luciferase reporter assay, real-time cell analysis and rescue experiment, co-localization analysis, RNA immunoprecipitation, and RNA pull down. The data showed that the three ncRNAs were predominant in the cytoplasm, and their regulatory patterns were focused on post-transcription. The fibrotic function of lnc949 depended on its host gene FKBP5. circ949 and circ057 formed a regulatory network with lnc865 and lnc556 to simultaneously regulate miR-29b-2-5p targeting STAT3 phosphorylation. Collectively, different RNAs can crosstalk with each other to regulate pulmonary fibrosis through different regulatory patterns. We hope these data can provide a full concept of RNA transcripts, leading to a new treatment for pulmonary fibrosis.

INTRODUCTION

High-throughput technologies, such as RNA sequencing, have revealed that only 2% of the transcribed genome codes are attributed to proteins. The remaining part of the transcribed genome is known as noncoding RNA (ncRNA).[1] Among the various types of ncRNAs, long ncRNA (lncRNA),[2] circular RNA (circRNA),[3] and microRNA (miRNA)[4] have attracted increasing attention. These ncRNAs are the upstream factors of mRNAs that directly or indirectly regulate the biological function of mRNAs[5] and play important roles in disease development. For example, lncBLACAT2 overexpression epigenetically induces intratumoral or peritumoral lymphangiogenesis and invasion of bladder cancer through a direct interaction with WDR5;[6] circRNA_100290 plays a role in oral cancer by targeting the miR-29 family;[7] and the miR-143/145 cluster is downregulated in colon cancer and other epithelial tumors.[8] With the wide-scale adoption of high-throughput sequencing techniques, these ncRNAs have been described as novel drug targets or biomarkers of various diseases, and they represent a potential research hotspot in the field of disease treatment. For instance, miR-150 is a potential biomarker associated with the prognosis and therapeutic outcome of colorectal cancer;[4] and targeting the liver-specific miR-122 by using an antisense-based approach is undergoing human trials for the treatment of the hepatitis C virus.[9] Therefore, understanding the regulation of these ncRNAs and their coding RNAs may provide clinically valuable predictive tools for effective treatments.

Pulmonary fibrosis is a specific form of chronic, progressive fibrosis of interstitial pneumonia characterized by lung scarring.[10] During the past decade, researchers have described many cellular and molecular mechanisms implicated in the pathogenesis of pulmonary fibrosis, aiming at identifying therapeutic targets. Unfortunately, the molecular mechanisms underlying the lung phenotype in pulmonary fibrosis are largely unknown.[11] Many miRNAs, including let-7d, miRNA-21, miRNA-29, miRNA-145, miRNA-200, and miRNA-199-5p, greatly influence pulmonary fibrosis.[12] In contrast to miRNAs, the role of considerably numerous lncRNAs and circRNAs in pulmonary fibrosis is poorly known. lncH19 mediates pulmonary fibrosis by

Received 11 April 2019; accepted 2 August 2019;
https://doi.org/10.1016/j.omtn.2019.08.018.

[4]These authors contributed equally to this work.

Correspondence: Xiaodong Song, Department of Cellular and Genetic Medicine, School of Pharmaceutical Sciences, Binzhou Medical University, No. 346, Guanhai Road, Laishan District, Yantai 264003, China.
E-mail: songxd71@163.com
Correspondence: Changjun Lv, Department of Cellular and Genetic Medicine, School of Pharmaceutical Sciences, Binzhou Medical University, No. 346, Guanhai Road, Laishan District, Yantai City, 264003, China.
E-mail: lucky_lcj@sina.com

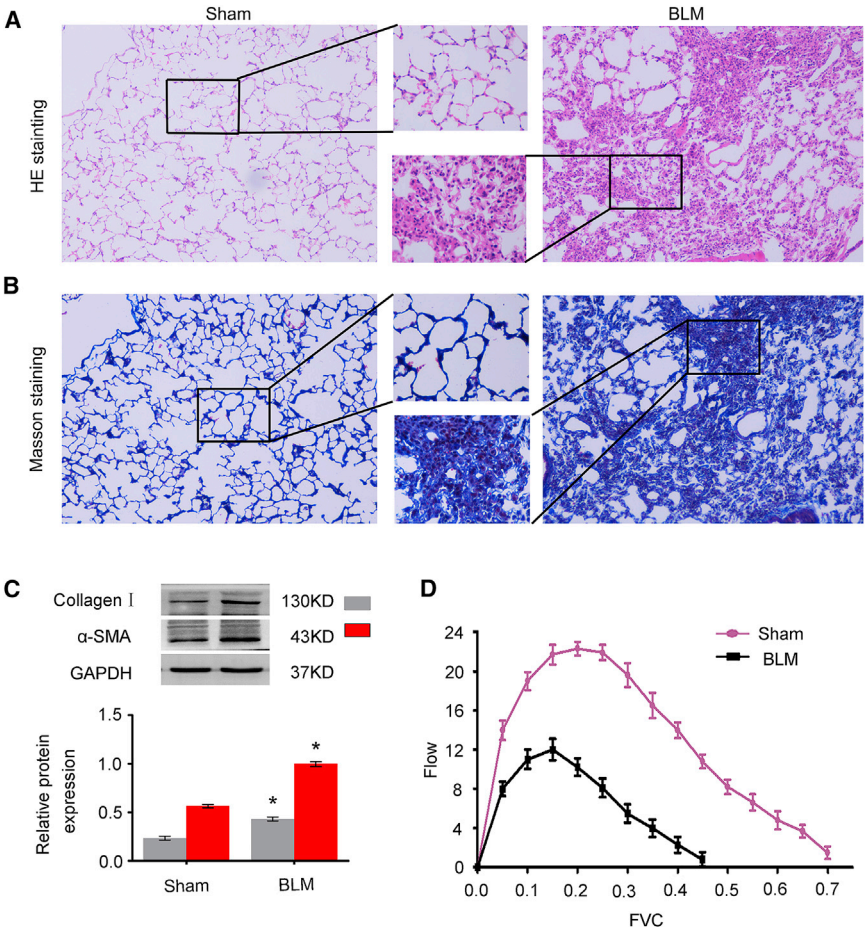

Figure 1. Identification of the BLM-Induced Mouse Model

(A) The BLM group had thicker alveolar walls compared with the sham group and showed strong immunohistochemical staining for collagens and collagen fibers, indicating that the hallmark of the fibroblastic foci was distinctly present. (B) Masson staining showed that the collagen matrix increased significantly in the BLM group and was accompanied by fibrosis lesion formation. Blue denotes the collagen in the interstitial lung. (C) The expression levels of collagen I and α-SMA significantly increased in the BLM group according to western blot analysis. (D) BLM decreased the FVC of mice in the BLM group compared with the sham mice. Each bar represents the mean ± SD, n = 6, *p < 0.05.

regulating the miRNA-196a/COL1A1 axis.[13] circHECTD is involved in the SiO_2-induced fibrosis by promoting endothelial cell migration and activation.[14] Therefore, these ncRNAs can be novel therapeutic targets for pulmonary fibrosis treatment. However, the data of these ncRNAs are sparse and nonsystematic, although the development of technologies has allowed an in-depth examination of these ncRNAs with unprecedented resolution and scale. Thus, systematically and comprehensively characterizing the crosstalk and regulatory pattern between ncRNAs and mRNAs can enhance our understanding of the pathogenesis of pulmonary fibrosis.

Our previous studies have reported the different RNA profiles in pulmonary fibrosis based on microarrays.[15–17] However, RNA sequencing is more sensitive in measuring differential RNA expression than microarrays. In the present study, we identified RNA transcripts using RNA sequencing in bleomycin (BLM)-induced mice. Combining RNA sequencing and other experimental data *in vivo* and *in vitro*, we analyzed and confirmed the crosstalk and regulatory pattern among these various types of RNAs, including mRNA, lncRNA, circRNA, and miRNA. We hope these data can provide a full concept of RNA transcripts in the pulmonary fibrosis field, leading to a new treatment for pulmonary fibrosis.

RESULTS

Pulmonary Fibrosis Evaluation in BLM-Induced Mice

H&E and Masson staining results revealed a well-defined pulmonary structure with integral air-blood barriers and low collagen levels in the sham group. In contrast, the BLM-treated mice pulmonary tissue structure was disordered, the air-blood barrier was severely damaged, the pulmonary interalveolar septum was thickened, and considerably numerous collagen fibers were deposited (Figures 1A and 1B). In line with these findings, the analysis of fibrotic markers, alpha sarcomeric actin (α-SMA) and collagen, revealed fibrosis formation (Figure 1C), leading to decrease in the forced vital capacity (FVC) compared with the sham mice (Figure 1D). Thus, the model of BLM-induced lung fibrosis was successfully established in mice.

Differentially Expressed mRNA, miRNA, and lncRNA

ncRNAs exert their regulatory functions through specific interactions with their target genes, that is, mRNAs. Thus, we first analyzed the differentially expressed mRNAs by RNA sequencing in BLM-induced lung fibrosis. Differentially expressed RNAs were identified by fold-change filtering, and the fold-change threshold was ≥ 3.0. Hierarchical clustering of mRNA analysis showed that differentially expressed 585 mRNAs were found in the BLM-induced models compared with those in the sham group (Figure 2A). Sequenced fragments further showed that the mRNA transcriptome changed globally in pulmonary fibrosis (Figure 2B). The number of exons had an extremely high variance from 1 to 35 (Figure 2C). Their length varieties were mainly within 2e + 05 (Figure 2D).

Then the differentially expressed miRNA were further analyzed. The analysis of the miRNA hierarchical clustering showed that 236 miRNAs were differentially expressed in the BLM-induced mice compared with those in the sham group (Figure 2E). Four upregulated

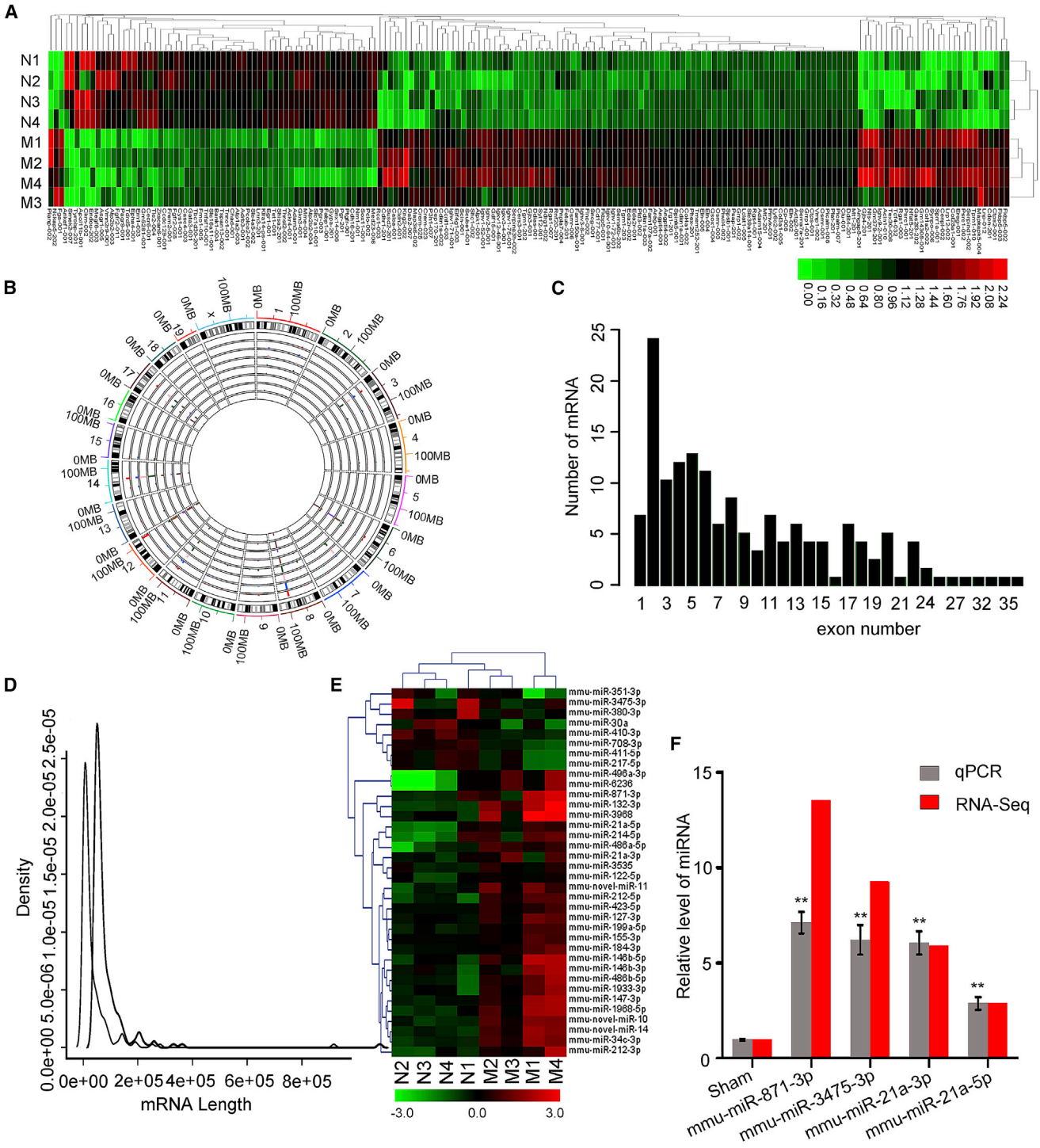

Figure 2. Differentially Expressed mRNAs and miRNAs by RNA Sequencing in BLM-Induced Lung Fibrosis

(A) Hierarchical clustering of mRNAs. Blue to red indicate the low-to-high expression levels. (B) Sequenced cDNA fragments mapped to chromosome, indicating that the RNA transcriptome changed globally. Each single circle represents a sample. (C) Number of exons per transcript for mRNA transcripts. (D) Length of mRNA. (E) Hierarchical clustering of miRNA analysis. (F) Results of quantitative real-time PCR and RNA sequencing showed that miR-21a-3p, miR-871-3p, miR-3475-3p, and miR-21a-5p were upregulated in BLM-induced lung fibrosis compared with those in the sham group. Each bar represents the mean ± SD, n = 6, **p < 0.01.

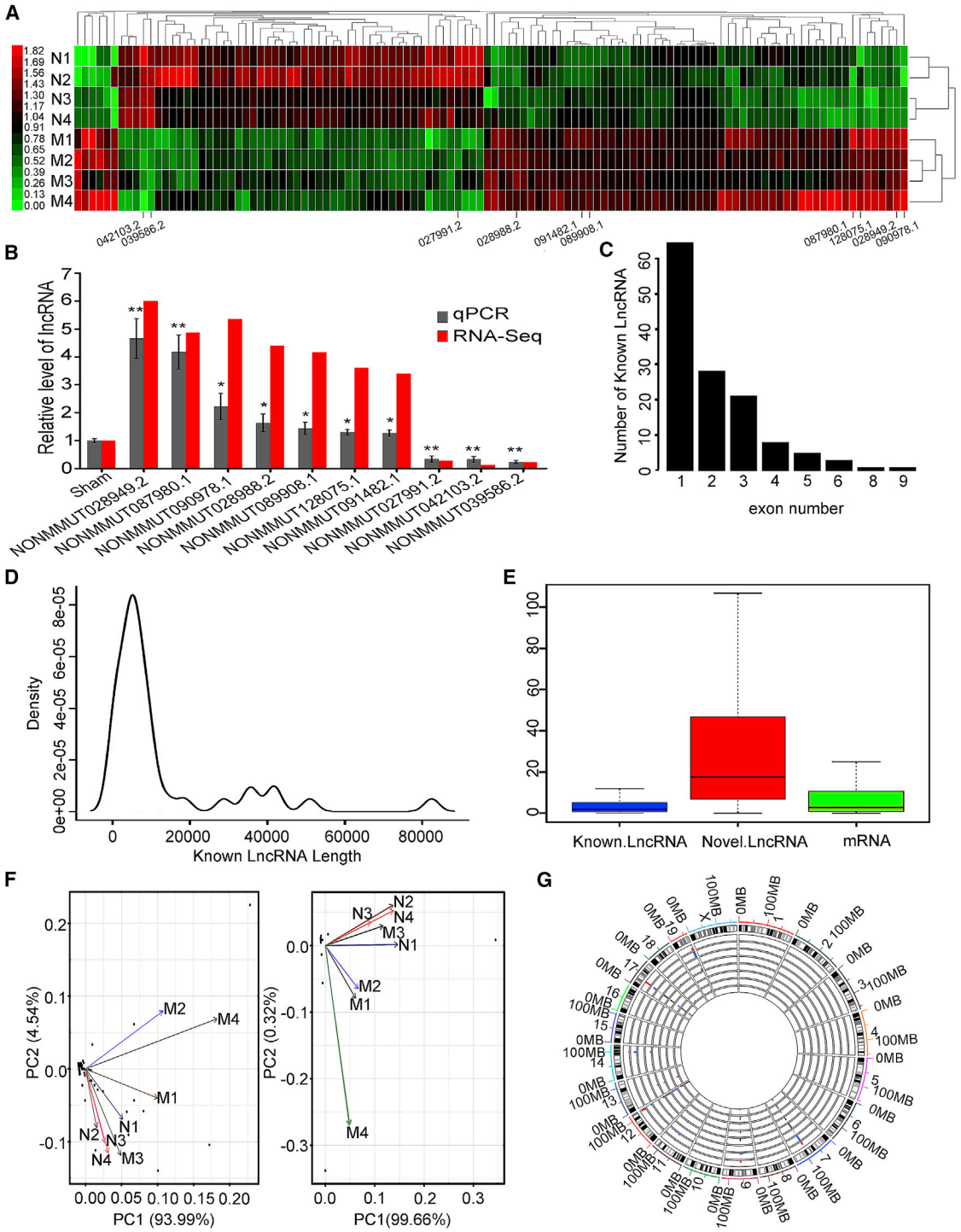

Figure 3. Differentially Expressed lncRNAs in BLM-Induced Lung Fibrosis

(A) Hierarchical clustering of lncRNAs. Blue to red indicate the low-to-high expression levels. (B) The lncRNAs of NONMMUT090978.1, NONMMUT028949.2, NONMMUT087980.1, NONMMUT028988.2, NONMMUT089908.1, NONMMUT128075.1, and NONMMUT091482.1 were upregulated, whereas NONMMUT027991.2, NONMMUT039586.2, and NONMMUT042103.2 were downregulated in BLM-induced lung fibrosis compared with those in the sham group, according to quantitative real-time PCR and RNA sequencing. Each bar represents the mean ± SD, n = 6, *$p < 0.05$, **$p < 0.01$. (C) Number of exons per transcript for all known lncRNA transcripts. (D) Distribution of transcript size for known lncRNA transcripts. (E) Expression of known lncRNA, novel lncRNA, and mRNA. (F) Principal component analysis (PCA) on all genes, lncRNAs, and mRNAs. (G) Circular representation of the genome-wide distribution of the expression of detected lncRNAs by RNA sequencing. Each single circle represents a sample.

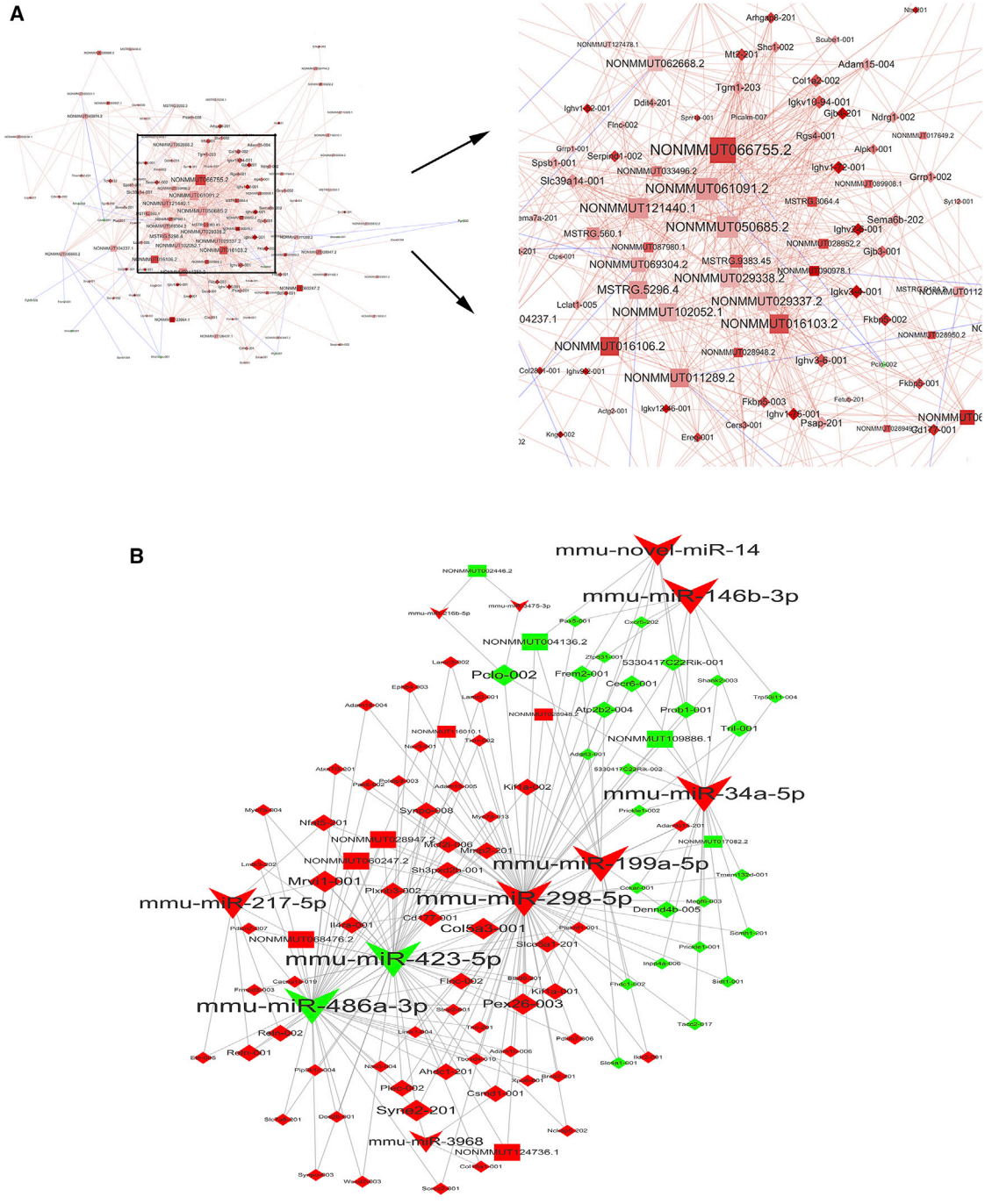

Figure 4. Interaction of Coexpressed mRNAs, miRNAs, and lncRNAs

(A) Interaction of coexpressed mRNA-lncRNA. (B) Interaction of coexpressed mRNA-miRNA-lncRNA. Upregulated RNAs are marked red. Downregulated RNAs are marked green. Diamond represents mRNAs. Arrow represents miRNA. Rectangle represents lncRNAs. Differentially expressed RNAs were identified by fold-change filtering, and the fold-change threshold was $\geq$ 4.0.

miRNA results were tested by quantitative real-time PCR to confirm the RNA sequencing data (Figure 2F). In the hierarchical clustering of lncRNAs, 272 lncRNAs were differentially expressed in the BLM-induced group compared with those in the sham group (Figure 3A). Furthermore, seven upregulated and three downregulated lncRNAs were tested by quantitative real-time PCR to validate the sequencing

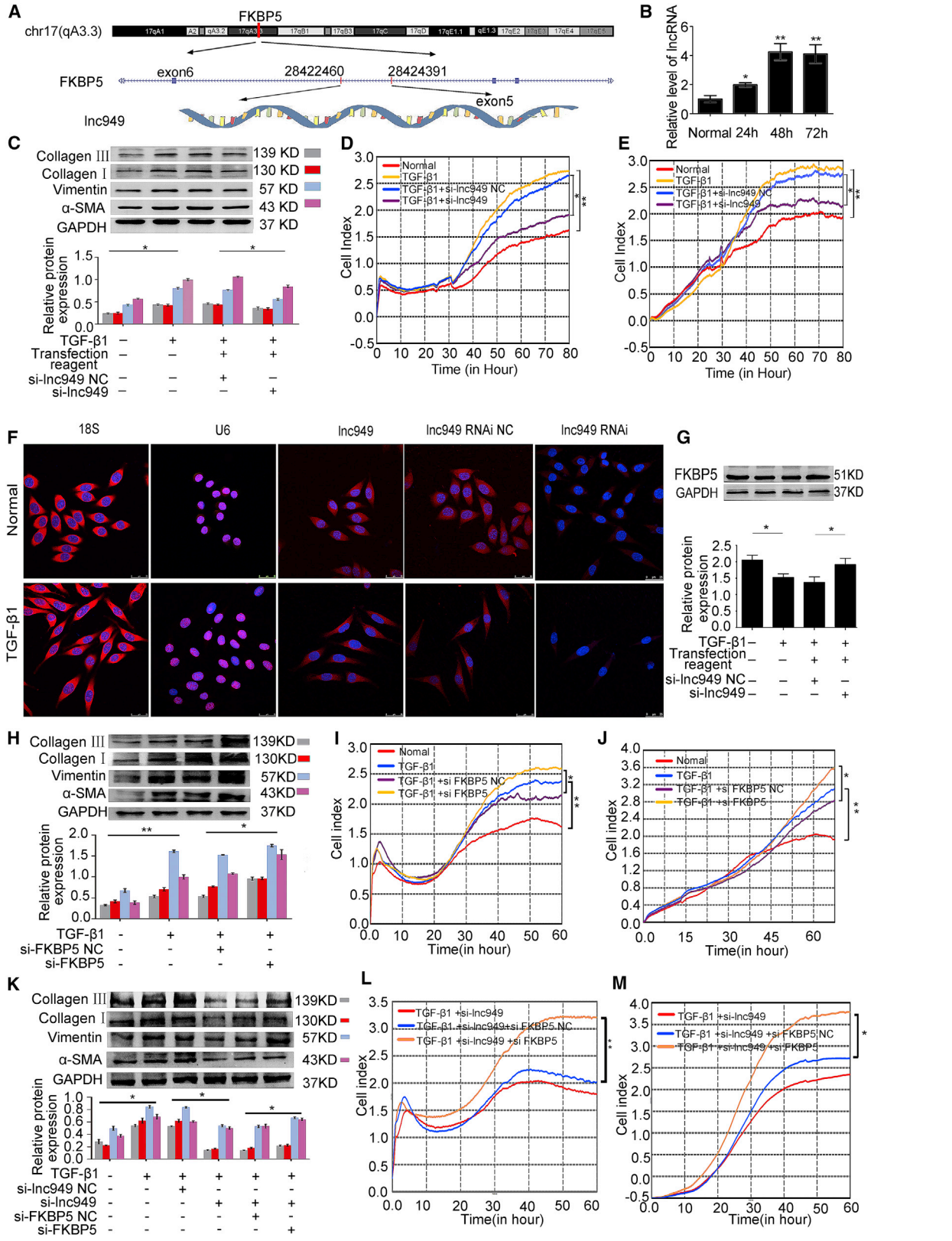

(legend on next page)

data. They were consistent with RNA sequencing in changing trends (Figure 3B). Next, these lncRNAs were analyzed from different perspectives. Most lncRNAs showed 1–4 exons, and their length varieties were mainly within 2,000 bp (Figures 3C and 3D). Specifically, these 272 lncRNAs, including 42 novel lncRNAs, were differentially expressed (Figure 3E). Sequenced fragments were mapped to the mouse genome, showing that lncRNAs changed globally in pulmonary fibrosis (Figures 3F and 3G); thus, a complex reprogramming of gene expression occurred during the fibrosis process.

Crosstalk of mRNA, miRNA, and lncRNA

Based on the above RNA sequencing data, the coexpressed mRNA, miRNA, and lncRNA interaction was analyzed. The interaction of coexpressed mRNA and lncRNA was first analyzed. A total of 131 mRNAs and 59 lncRNAs coexpressed in the BLM-induced models compared with those in the sham group (Figure 4A). The coexpressed mRNA-miRNA-lncRNA interaction was further analyzed based on the above interaction of coexpressed mRNA-lncRNA. A total of 85 mRNAs, 11 miRNAs, and 10 lncRNAs coexpressed and interacted with one another (Figure 4B).

Crosstalk of lnc949 and Its Host Gene FKBP5

Many ncRNAs intersect in protein-coding loci or come from their protein-coding genes, namely, host genes. Thus, ncRNAs exhibited a strong pattern of coexpression with their host genes. lncRNA-NONMMUT028949.2 (lnc949) was chosen as an example to study the regulatory pattern among ncRNA and host gene crosstalk because it had the highest expression. lnc949 was located in chromosome 17 in the genome. Its transcription was mapped in the intron of its host gene recombinant FK506 binding protein 5 (FKBP5) from 28,422,460 to 28,424,391 (Figure 5A). Its sequence was analyzed using the open reading frame finder from the National Center for Biotechnology Information (NCBI). A protein in more than 90 amino acids failed to predict. The amino acid sequences for the conserved domains from NCBI were searched and found that lnc949 did not contain a valid Kozak sequence, indicating that lnc949 has no protein-coding potential. Then, quantitative real-time PCR was used to analyze lnc949 expression in L929, a fibroblast cell line. lnc949 was upregulated in L929 cells treated with transforming growth factor β1 (TGF-β1) for 24, 48, and 72 h (Figure 5B), conforming to the results obtained from animal models. Therefore, L929 was used as a cell model to further study lnc949 function and mechanism.

Fundamental characteristics of pulmonary fibrosis included the manifestations of mesenchymal markers, uncontrolled proliferation, and high migration rates in lung cell. Thus, small RNA interference on lnc949 (si-lnc949) was designed to test lnc949 function in fibrosis process. Western blot results showed that the mesenchymal markers, such as α-SMA, vimentin, and collagen, decreased after lnc949 interference (Figure 5C). Results of real-time proliferation and migration analysis system showed that si-lnc949 inhibited cell proliferation and migration (Figures 5D and 5E). lncRNA regulates host gene via transcriptional or post-transcriptional pattern. The former process generally happens in the nucleus, whereas the latter happened in the cytoplasm. Thus, we examined lnc949 localization by performing RNA fluorescence *in situ* hybridization (FISH). Data showed that lnc949 was predominant in cytoplasm (Figure 5F), indicating that lnc949 regulated its host gene FKBP5 mainly via post-transcription. Western blot results showed that FKBP5 expression increased after lnc949 interference (Figure 5G). Meanwhile, after FKBP5 interference (si-FKBP5) the expression of α-SMA, vimentin, and collagen increased, and cell proliferation and migration also increased (Figures 5H–5J). A rescue experiment was carried out to further confirm these findings. After the samples were co-treated with si-lnc949 and si-FKBP5, we found that si-FKBP5 reversed the effect of si-lnc949 treatment (Figure 5K). Meanwhile, the proliferation and migration of samples co-treated with si-lnc949 and si-FKBP5 were also detected. The results were consistent with the rescue experiment (Figures 5L and 5M). The findings suggest that the fibrotic function of lnc949 depended on its host gene FKBP5.

Crosstalk of ncRNAs and Their Targeted Gene

All types of RNA transcripts can crosstalk with each other by binding their targeted genes.[18] lncPCF regulated map3k11 through binding to miR-344a-5p to promote pulmonary fibrosis in our previous study;[16] therefore, circRNA was chosen to further prove this regulatory pattern in this study. The differentially expressed circRNAs were tested by RNA-sequencing in the BLM-induced mice. Hierarchical clustering results showed that 74 circRNAs were differentially expressed in BLM-induced lung fibrosis compared with those in the sham group (Figure 6A). Sequenced fragments were mapped to the mouse genome, showing that circRNAs changed globally in pulmonary fibrosis (Figures 6B and 6C). Upregulated circRNA14:30346797-30350949 (circ949) and 6:99003199-99100057 (circ057) were tested by quantitative real-time PCR to validate the sequencing data (Figure 6D). The circular junction of circ949 and circ057 was identified using divergent primers on Sanger sequencing (Figures 6E and 6F). The results showed that circ949 was formed by the circularization of the sequence of 2–3 exons in CACNA1D gene, and its length was 416

Figure 5. lnc949 Promoted Pulmonary Fibrosis through Regulating Its Host Gene FKBP5 Post-transcription

(A) lnc949 was mapped to chromosome 17 and located in the fifth intron of the FKBP5 gene. (B) lnc949 increased in L929 cells treated with TGF-β1 for 24, 48, and 72 h compared with those in the normal cell. (C) Collagen, vimentin, and α-SMA decreased under si-lnc949 action by western blot. (D) si-lnc949 inhibited the TGF-β1-treated cell proliferation tested by real-time cell analysis system. (E) si-lnc949 inhibited the TGF-β1-treated cell migration tested by a real-time cell analysis system. (F) RNA-FISH showed that lnc949 was predominant in the cytoplasm. (G) FKBP5 decreased in pulmonary fibrosis. After lnc949 interference, FKBP5 increased. (H) Collagen, vimentin, and α-SMA increased under si-FKBP5 action by western blot. (I) si-FKBP5 promoted the TGF-β1-treated cell proliferation. (J) si-FKBP5 promoted the TGF-β1-treated cell migration. (K) Rescue experiment showed that si-lnc949 reduced the expression of the fibrotic indicators collagen, vimentin, and α-SMA, and si-FKBP5 reversed this effect of si-lnc949. (L) Real-time cell proliferation system observed that si-lnc949 inhibited the cell proliferation. si-FKBP5 reversed this effect of si-lnc949. (M) Real-time cell proliferation system observed that si-lnc949 blocked the cell migration. si-FKBP5 reversed this effect of si-lnc949. Each bar represents the mean ± SD, n = 6, *p < 0.05, **p < 0.01.

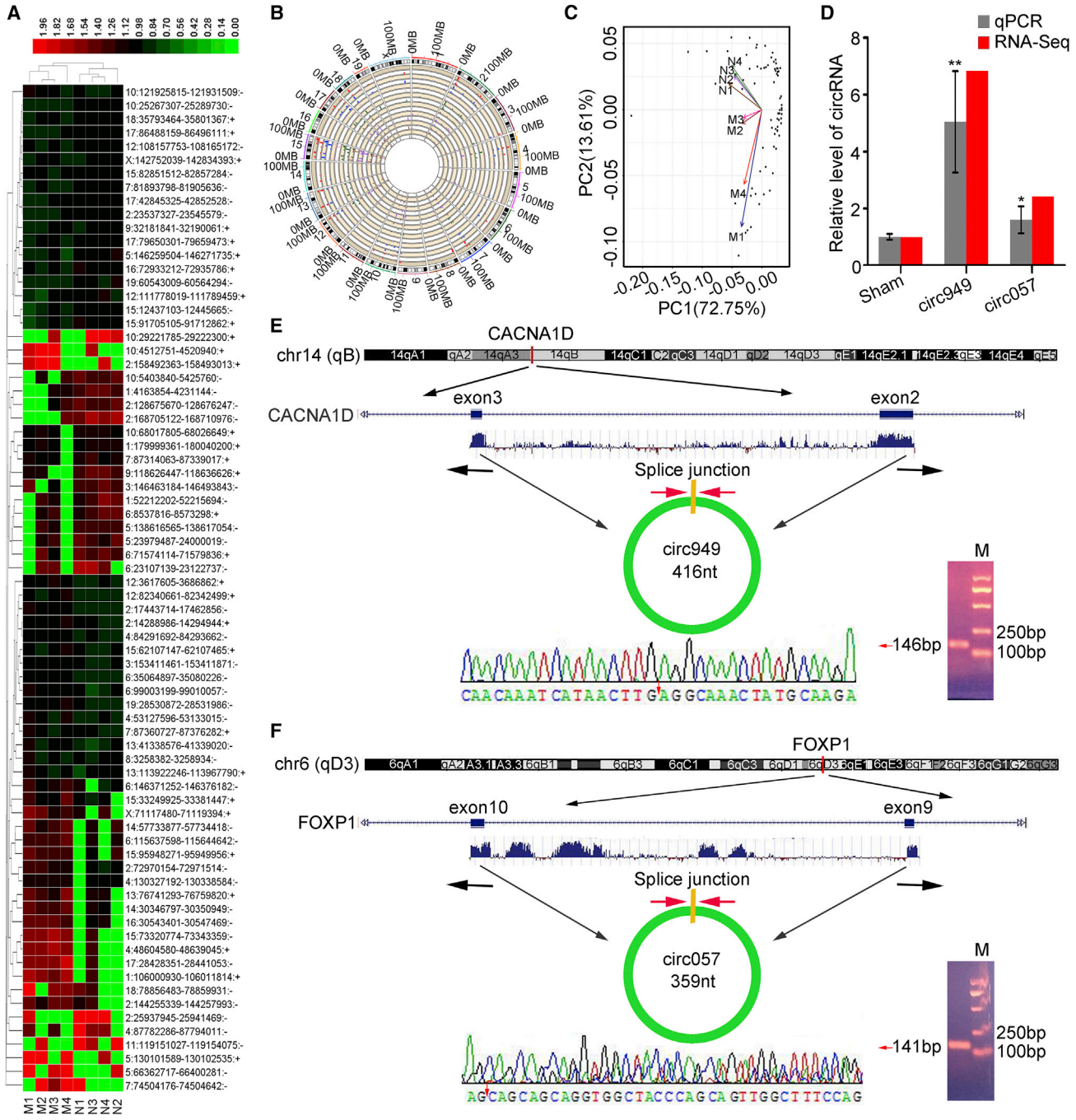

Figure 6. Differentially Expressed circRNAs in BLM-Induced Lung Fibrosis

(A) Hierarchical clustering of circRNAs analysis. (B) Differentially expressed circRNAs mapped to chromosome. Each single circle represents a sample. (C) PCA on each sample. (D) circ949 and circ057 were upregulated in BLM-induced lung fibrosis compared with those in the sham group, according to quantitative real-time PCR and RNA sequencing. Each bar represents the mean ± SD, n = 6, *$p < 0.05$, **$p < 0.01$. (E) Circular junction of circ949 from CACNA1D gene was identified using divergent primers on Sanger sequencing. (F) Circular junction of circ057 from FOXP1 gene was identified using divergent primers on Sanger sequencing.

nt. The circ057 were formed by the circularization of the sequence of 9–10 exons in FOXP1 gene, and its length was 359 nt. circ949 and circ057 locations were tested by RNA-FISH, which showed that circ949 and circ057 were predominant in the cytoplasm (Figure 7A), indicating that their regulation on targeted genes might be focused on post-transcription.

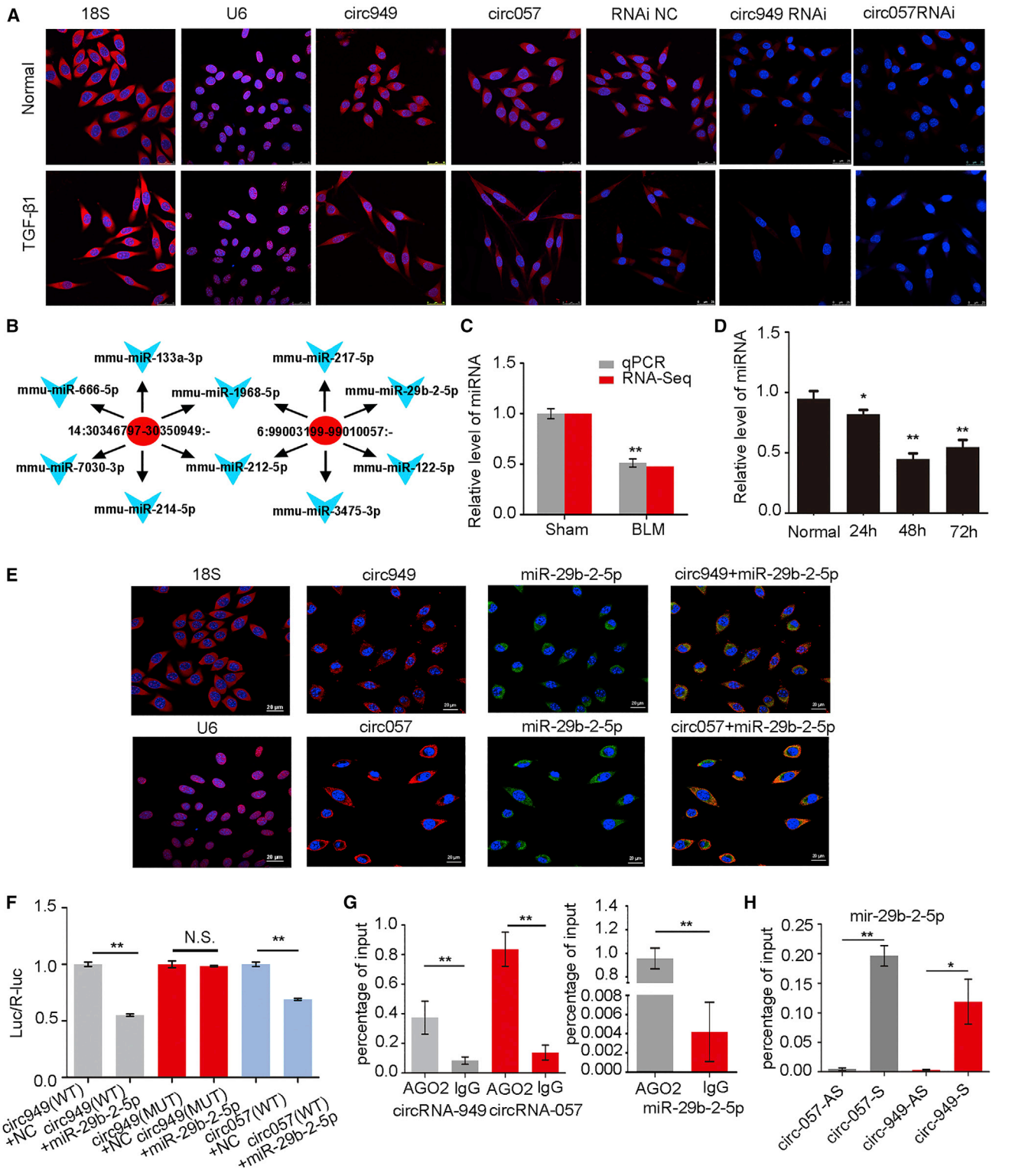

Figure 7. A Regulatory RNA Network Involving miR-29b-2-5p, circ949, and circ057

(A) RNA-FISH showed that circ949 and circ057 were predominant in the cytoplasm. (B) Analysis of the binding sites of circ949 and circ057 for the miRNAs. (C) miR-29b-2-5p expression decreased as observed using RNA-sequencing and quantitative real-time PCR methods. (D) miR-29b-2-5p decreased in L929 cells treated with TGF-β1 for 24,

(legend continued on next page)

Then, as previously described,[15] miRNA binding-site prediction in circRNA was based on their full-length sequences. Six miRNAs were found binding to circ949 and circ057 (Figure 7B). Among these miRNAs, circ949 and circ057 simultaneously targeted miR-29b-2-5p and had higher binding scores than others. Thus, miR-29b-2-5p was selected for further study. RNA sequencing and quantitative real-time PCR results showed that miR-29b-2-5p was decreased in BLM-induced lung fibrosis compared with that in the sham group (Figure 7C). Meanwhile, miR-29b-2-5p was decreased in L929 cells treated with TGF-β1 for 24, 48, and 72 h (Figure 7D).

The immunofluorescence double-labeling experiment showed colocalization of circ949 and miR-29b-2-5p as well as circ057 and miR-29b-2-5p (Figure 7E). Dual-luciferase report system was constructed to verify the direct targeted relationship between miR-29b-2-5p and circ949/circ057. The data showed that miR-29b-2-5p was a direct targeted miRNA for both circ949 and circ057 (Figure 7F). RNA immunoprecipitation (RIP) and RNA pull-down experiments were performed to the directly targeted relationship between circ949 and miR-29b-2-5p, and circ057 and miR-29b-2-5p (Figures 7G and 7H).

Then, the targeted lncRNAs of miR-29b-2-5p were further analyzed. lncRNA-NONMMUT039556 (lnc556) and NONMMUT039865 (lnc865) were predicted to have binding sites for miR-29b-2-5p. RNA sequencing and quantitative real-time PCR results indicated that lnc865 and lnc556 expression were increased *in vivo* (Figure 8A), indicating lnc865 and lnc556 were potential target genes for miR-29b-2-5p. Dual-luciferase report system confirmed the direct targeted relationship that the miR-29b-2-5p was also a targeted miRNA for both lnc865 and lnc556 (Figure 8B).

Finally, miR-29b-2-5p targeted mRNAs were predicted on the basis of TargetScan, miRanda data, and miRbase. Among the listed miR-29b-2-5p-targeted genes, we focused on STAT3 and Gli2 because they were the master regulatory factors of lung fibrosis in our previous study.[19,20] The data showed that miR-29b-2-5p mimic inhibited the expression of luciferase combined with the 3′ UTR of STAT3 but cannot inhibit the expression of luciferase combined with 3′ UTR of Gli2, indicating that STAT3 was the targeted gene for miR-29b-2-5p (Figure 8C). Therefore, miR-29b-2-5p gain- and loss-of-function studies were performed to investigate the mechanism of them. Western blot results showed that miR-29b-2-5p mimic inhibited STAT3 and p-STAT3 expression, whereas miR-29b-2-5p inhibitor promoted STAT3 and p-STAT3 expression, indicating STAT3 phosphorylation plays roles in signal transduction (Figure 8D).

It is very interesting that miR-29b-2-5p is these RNAs regulatory center (Figure 8E), so miR-29b-2-5p function was explored in depth (Figures 8F–8H). The gain- and loss-of-function experiments showed that miR-29b-2-5p mimic inhibited α-SMA, vimentin, and collagen expression, and blocked the proliferation and migration of cells treated with TGF-β1. Conversely, miR-29b-2-5p inhibitor increased α-SMA, vimentin, and collagen expression and promoted the cell proliferation and migration. All these fundings indicate that various types of RNAs, including mRNA, miRNA, lncRNA, and circRNA, can crosstalk with each other, forming the complicated regulation network to mediate the pulmonary fibrosis development.

DISCUSSION

In the past decade, researchers have identified many therapies used in pulmonary fibrosis treatment. However, only a few treatments can increase the survival rates and improve the quality of the patients' life. This situation is attributed to complex regulatory network of pulmonary fibrosis, thereby relating to multiple genes and pathways.[21] Therefore, targeting multiple genes is likely to be the future direction of the disease treatment. In the present study, we applied RNA sequencing and related experiments to examine various kinds of RNA crosstalk and their regulatory pattern in pulmonary fibrosis, which represents novel therapeutic direction for pulmonary fibrosis treatment.

Whole-transcriptome RNA sequencing has revealed considerably numerous novel genes in human genome in recent years. Most of these novel genes are ncRNAs.[22] ncRNAs do not possess the coding-protein feature. Nevertheless, they serve important functions in various life activities.[23] Dysfunction of ncRNA is a primary characteristic associated with various complex human diseases, such as psoriasis, Alzheimer's disease, spinocerebellar ataxia, prostate cancer, and leukemia.[24–26] Our data showed that pulmonary fibrosis involved many dysfunctional ncRNAs. Each ncRNA regulated a broad spectrum of target genes and affected many signaling pathways. Disruption of a single ncRNA may only limit an inhibitory effect, whereas joint interference of multiple ncRNAs may be more effective. Based on this principle, an interfering lncRNA targeting multiple miRNAs was designed and subjected to trials for hepatocellular carcinoma (HCC) treatment.[27] Considering the high abundance of ncRNAs and frequent promiscuity of protein-RNA interactions, many mutual regulatory modes, such as methylation, histone modification, and transcription factor recruitment, exist between ncRNAs and mRNAs.[28–31] The two regulatory patterns in the crosstalk of ncRNAs with their host genes and targeted genes were chosen as examples for further research in this study.

Many ncRNAs intersect in their host gene loci or come from their host genes, so ncRNA regulates its host gene as an important

48, and 72 h compared with those in the normal cell. (E) The immunofluorescence double-labeling experiments showed the existence of two-gene co-localized phenomenon, including circ949 and miR-29b-2-5p, and circ057 and miR-29b-2-5p. (F) Firefly and Renilla dual-luciferase report showed that miR-29b-2-5p inhibited luciferase activity combined with circ949 and circ057, but miR-29b-2-5p cannot inhibit luciferase activity combined with circ949 mutation. (G) RIP assay identified that circ949 and miR-29b-2-5p and circ057 and miR-29b-2-5p were significantly enriched in Ago2-containing beads compared to the input group. (H) Biotin-labeled miRNA pull-down assay demonstrated that miR-29b-2-5p could bind circ949 and circ057. Each bar represents the mean ± SD, n = 6, *p < 0.05, **p < 0.01.

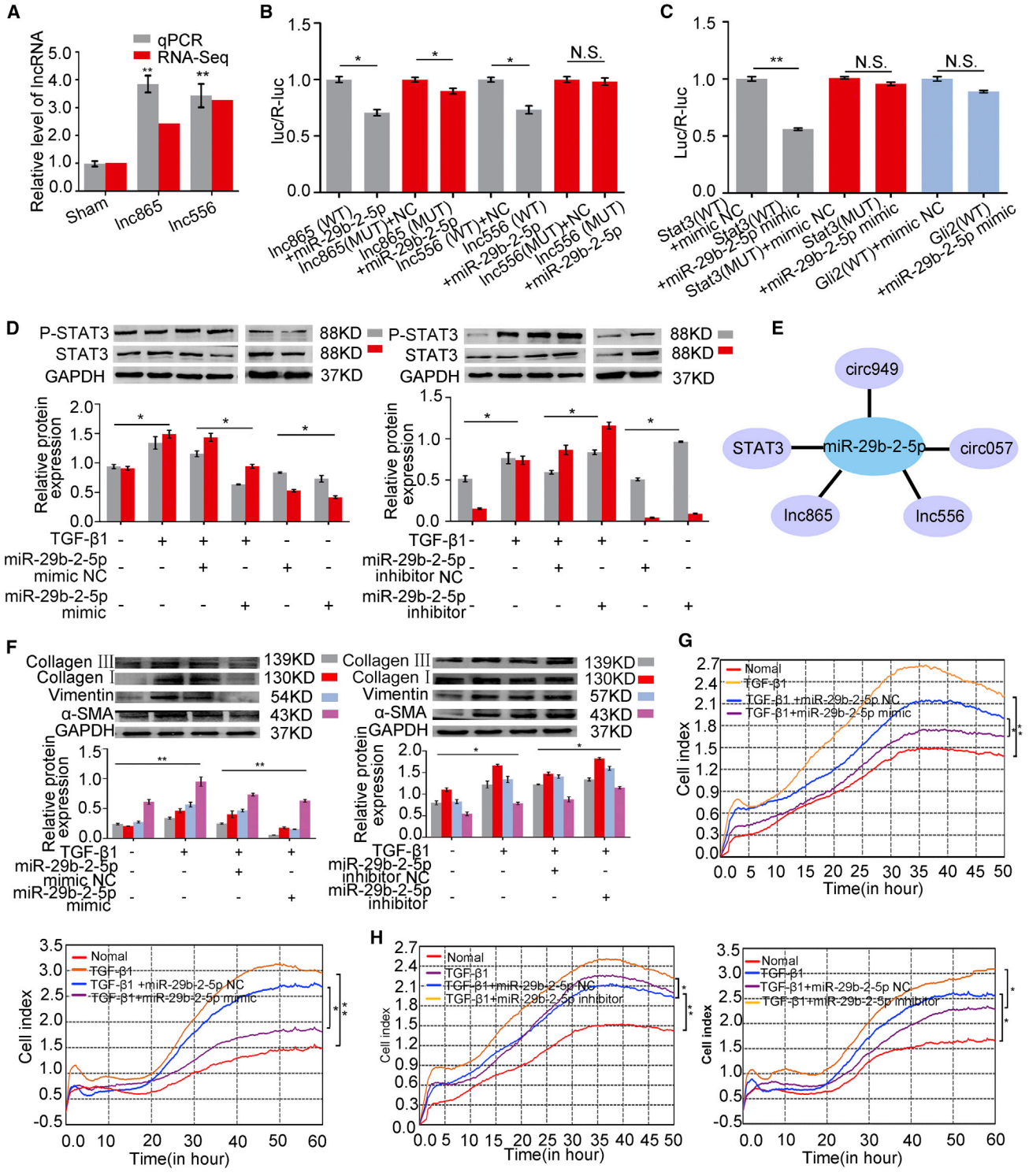

Figure 8. A Regulatory RNA Network Involving miR-29b-2-5p, lnc865, lnc556, and STAT3

(A) RNA sequencing and quantitative real-time PCR results indicated that lnc865 and lnc556 expression increased in BLM-induced lung fibrosis. (B) Firefly and Renilla dual-luciferase report showed that miR-29b-2-5p inhibited luciferase activity combined with lnc865 and lnc556. (C) Firefly and Renilla dual-luciferase report showed that miR-

(legend continued on next page)

regulatory pattern between ncRNA and mRNA.[32,33] In many cases, lncRNA transcriptions may positively or negatively affect the expression of their host genes by regulating the host genes to exert their function. For example, circZKSCAN1 and its host gene ZKSCAN1 cooperate closely with one another to inhibit growth, migration, and invasion of human HCC, which may be a useful marker for HCC diagnosis.[34] lncITPF promotes pulmonary fibrosis by targeting heterogenous nuclear rib onconucleoprotein (hnRNP)-L depending on its host gene ITGBL1.[17] In this study, lnc949 regulated its host gene FKBP5 through the post-transcription pattern in *cis*-regulation. Certainly, experiments will be designed to determine this pattern in future research.

The second regulatory pattern is that all types of RNA transcripts crosstalk with each other through regulating their targeted genes. For example, lncMD1 targets miR-133 and miR-135 to control muscle differentiation.[35] The networks of circRNA that targeted miRNA through regulating Hmgb2 and Dio2 are systematically dissected in the brain of senescence-accelerated mouse.[36] lncPFL contributes to cardiac fibrosis by targeting let-7d.[37] In a recent report, a lncRNA, a circRNA, and two miRNAs formed a regulatory RNA network in the mammalian brain. The lncRNA Cyrano represses a mRNA via target-directed miRNA degradation, thereby enabling the accumulation of the circRNA Cdr1as.[38] This study listed many ncRNAs, which might bind to miRNAs to regulate pulmonary fibrosis progress. Meanwhile, this study also thoroughly explored two lncRNAs, two circRNAs, a miRNA, and a mRNA forming a regulatory RNA network, in which circ949, circ057, lnc865, and lnc556 coordinates regulated the same miR-29b-2-5p targeting STAT3 to control pulmonary fibrosis. Our data will serve as useful resources for developing therapeutic targets or novel diagnostics for fibrosis treatment in the future.

Certainly, other regulatory patterns were present in these RNAs. For example, some miRNAs originate from lncRNA.[39] In some cases, ncRNA can act as a protein-coding gene.[40] Occasionally, ncRNA acts as both protein-coding gene and ncRNA.[41] These different regulations reflect the diversity and complexity of crosstalk and regulatory pattern among these different types of RNAs.

An increasing number of ncRNAs have been discovered in recent years. Detecting alterations in ncRNAs has quickly become a hot research area. In these cases, methods for ncRNA detection have rapidly developed. As an analysis technique, the method of surface-enhanced Raman spectroscopy (SERS) has currently developed rapidly. SERS is an ideal tool for analyzing biological samples including viruses, bacteria, proteins, and nucleic acids, because of its high sensitivity and specificity on the basis of the principle of Raman effect. SERS does not require nucleic acid amplification when rapidly and accurately detecting ncRNA; this method is more convenient to use for ncRNA detection. Driskell et al.[42] have reported that SERS can be used to detect ncRNA. Thus, a detailed information on the regulatory patterns of these RNA crosstalks will be explored in the future.

In conclusion, the present study provides a more systematic and comprehensive regulation among various RNA crosstalks in pulmonary fibrosis. These findings may provide mechanisms, possible biomarkers, and novel treatment for pulmonary fibrosis.

MATERIALS AND METHODS

Animal Model and Ethics Statement

Eight-week-old C57BL/6 mice were obtained from the Model Animal Research Center of Nanjing University (Nanjing, China). All animal experiments were performed according to regulations established by the Ethics Committee on Animal Experiments of Binzhou Medical University. Mice were randomly divided into two groups (10 mice each): the sham control and lung fibrosis model group. Pulmonary fibrosis mice were administered with 5 mg/kg saline-dissolved BLM via single intratracheal instillation under anesthesia. Sham control mice received an equal volume of saline only. Lung tissues were harvested on the 28th day following treatment with BLM. Histopathological changes and collagen deposition were assessed by the H&E and Masson staining as our previously described.[15]

RNA Sequencing

2 μg RNA was used as input material for the RNA sample preparations. Sequencing libraries were generated following the manufacturer's recommendations. The detailed procedure is given as previously described.[17]

Cell Model and Treatment

Mouse lung fibroblast cell line L929 were purchased from the Cell Bank of the Chinese Academy of Sciences. The cells were maintained in advanced minimum essential medium and supplemented with 10% newborn calf serum, 100 U/mL penicillin, and 100 μg/mL streptomycin at 37°C under a humidified atmosphere of 5% CO_2 and 95% air. The cells were administered with 5 ng/mL TGF-β1.

Western Blot

Protein concentration was quantified using a bicinchoninic acid protein assay kit and boiled with the sample buffer in a water bath for 5 min. Protein samples were separated with 15% SDS-PAGE gels

29b-2-5p mimic inhibited the activity of luciferase combined with the 3′ UTR of STAT3. The activity of luciferase increased again after the binding site mutation. Furthermore, miR-29b-2-5p mimic cannot inhibit the activity of luciferase combined with the 3′ UTR of Gli2. (D) STAT3 and p-STAT3 decreased under miR-29b-2-5p mimic action, whereas it increased under miR-29b-2-5p inhibitor action. (E) Circ949 and circ057, lnc865 and lnc556, and STAT3 and miR-29b-2-5p formed a regulatory network to control fibrosis. (F) miR-29b-2-5p mimic inhibited the expression of collagen, vimentin, and α-SMA, but miR-29b-2-5p inhibitor promoted the expression of collagen, vimentin, and α-SMA. (G) miR-29b-2-5p mimic blocked the TGF-β1-treated cell proliferation and migration. (H) miR-29b-2-5p inhibitor enhanced the TGF-β1-treated cell proliferation and migration. Each bar represents the mean ± SD, n = 6, *$p < 0.05$, **$p < 0.01$.

Table 1. Primers Used in Quantitative Real-Time PCR

Name		Sequence
NONMMUT028949.2	sense	5′-GGTGAGCATTGGTCAGCAAG-3′
	anti-sense	5′-CGCACGCCTCTCCTCTAACT-3′
NONMMUT087980.1	sense	5′-CTGTGTGGCTAGACCTGGAATC-3′
	anti-sense	5′-GGCTTGAAGCACACGGTAATC-3′
NONMMUT090978.1	sense	5′-CCTCATGACCAAACCCTTCAC-3′
	anti-sense	5′-GGTCGGTGGAGGAGTATGAAAC-3′
NONMMUT028988.2	sense	5′-GAAACAGGGCACTTGGTTCA-3′
	anti-sense	5′-GCTTCGGCGAGTCTATCTAGAG-3′
NONMMUT089908.1	sense	5′-CCTGCTTGTCTGCACATAGTGG-3′
	anti-sense	5′-GCGTTAGTCAGCCATTGGTCA-3′
NONMMUT128075.1	sense	5′-AGGTACACGCTGTGCCAAAC-3′
	anti-sense	5′-CGGAGATTCGGTTCCTGCT-3′
NONMMUT091482.1	sense	5′-GAGCGAAGGTCACTCGTTCA-3′
	anti-sense	5′-CTCTGAGACAAAACTTGGCACA-3′
NONMMUT027991.2	sense	5′-CTAGCCATAAACGTATTTCACCATC-3′
	anti-sense	5′-GCTCCATCTGTACAGGACTCTCTC-3′
NONMMUT042103.2	sense	5′-GGTGCTCAGTGTTCAAGAACCA-3′
	anti-sense	5′-ACGTCATGATCACGCCTTCTC-3′
NONMMUT039586.2	sense	5′-GGAGCGTCTCACCACTGGAA-3′
	anti-sense	5′-CAGCATTTTCACGAATGACTTG-3′
circ057	sense	5′-GCATGCCTCTACCAATGGACAG-3′
	anti-sense	5′-CTGGAGAGACAAGAGGTGCTGC-3′
circ949	sense	5′-GCATTAGTATAGTGGAATGGAAACC-3′
	anti-sense	5′-CTCTTGCATAGTTTGCCTCAAGT-3′
lnc556	sense	5′-GACAGTTAGCTTTATTTGGCACTG-3′
	anti-sense	5′-GCTTCCTTGTTCTTGTCACCAC-3′
lnc856	sense	5′-AGATGGGAGCAATATAGTATGATCC-3′
	anti-sense	5′-ACTGTCTATGACTACCCATGAGTCC-3′

for 2 h and transferred onto a polyvinylidene difluoride membrane, which was subsequently blocked in 5% non-fat milk for 2 h. Blots were probed using the primary antibodies. After three times washing with tris buffered saline tween, the horseradish peroxidase-conjugated secondary antibodies were added. Antigen-antibody complexes were visualized by enhanced chemiluminescence.

Quantitative Real-Time PCR

Total RNA was isolated using TRIzol reagent (Invitrogen, USA). RNA quantity and quality were measured using the NanoDrop 2000 spectrophotometer (Thermo Scientific, USA) and RNA integrity was assessed by standard denaturing agarose gel electrophoresis. Complementary DNA synthesis was performed using the M-MLV reverse transcriptase kit (Invitrogen, USA) following the manufacturer`s instructions. Quantitative real-time PCR was performed using a SYBR green-based PCR master mix kit (Takara, Japan) on a Rotor Gene 3000 real-time PCR system. Primers used in quantitative real-time PCR are shown in Table 1.

Single-Molecule RNA FISH Detection

FISH probe on lnc949, circ949, and circ057 was synthesized, and the steps were performed by using the FISH kit according to the manufacturer's protocol (RiboBio Technology). In brief, cells were fixed with 4% paraformaldehyde, permeabilized in PBS with 0.5% Triton X-100, followed by pretreatment with prehybridization buffer. Cells were then hybridized with 0.5 μM Cy3-labeled RNA of lnc949, circ949, and circ057 or U6/18S FISH probe mix overnight. After hybridization, cells were stained with DAPI. The images were observed and analyzed with a confocal microscope (Leica, Germany).

Real-Time Cellular Proliferation and Migration Analyses

4×10^5 cells proliferation and migration were analyzed in E-plate (proliferation plate) and CIM plate (migration plate) in a real-time cellular analysis DPlus instrument, which can automatically record proliferation and migration curves. Cell index representing the amount of proliferating or migrating cells was calculated by using

real-time cellular analysis from ACEA Biosciences (ACEA Biosciences, China), as previously described in a study.[16]

Statistical Analysis

Data are expressed as the mean ± SD, and statistical significance was assessed by unpaired Student's t test for experiments comparing two groups, whereas one-way ANOVA with Student-Newman-Keuls post hoc test was applied for experiments comparing three or more groups. Probability values of less than 0.05 were considered significant. Statistical analyses were performed using SPSS version 19.0 software.

AUTHOR CONTRIBUTIONS

C. Li, Z.W., and J.Z. performed experiments and analyzed data. X.Z., P.X., and X.L. contributed to animal experiments and data analysis. M.L., C. Lv, and X.S. contributed to the initial experimental design and wrote the paper.

CONFLICTS OF INTEREST

The authors declare no competing interests.

ACKNOWLEDGMENTS

This study was supported by the National Natural Science Foundation of China (81870001, 81741170, 81670064, and 31670365), the Important Project of Research and Development of Shandong Province (2018GSF121018), and the Natural Science Foundation of Shandong Province (ZR2018PH001).

REFERENCES

1. Trapnell, C., Williams, B.A., Pertea, G., Mortazavi, A., Kwan, G., van Baren, M.J., Salzberg, S.L., Wold, B.J., and Pachter, L. (2010). Transcript assembly and quantification by RNA-Seq reveals unannotated transcripts and isoform switching during cell differentiation. Nat. Biotechnol. *28*, 511–515.

2. Meng, L., Ward, A.J., Chun, S., Bennett, C.F., Beaudet, A.L., and Rigo, F. (2015). Towards a therapy for Angelman syndrome by targeting a long non-coding RNA. Nature *518*, 409–412.

3. Li, Y., Zheng, F., Xiao, X., Xie, F., Tao, D., Huang, C., Liu, D., Wang, M., Wang, L., Zeng, F., and Jiang, G. (2017). CircHIPK3 sponges miR-558 to suppress heparanase expression in bladder cancer cells. EMBO Rep. *18*, 1646–1659.

4. Ma, Y., Zhang, P., Wang, F., Zhang, H., Yang, J., Peng, J., Liu, W., and Qin, H. (2012). miR-150 as a potential biomarker associated with prognosis and therapeutic outcome in colorectal cancer. Gut *61*, 1447–1453.

5. Liu, Y., Guo, R., Hao, G., Xiao, J., Bao, Y., Zhou, J., Chen, Q., and Wei, X. (2015). The expression profiling and ontology analysis of noncoding RNAs in peritoneal fibrosis induced by peritoneal dialysis fluid. Gene *564*, 210–219.

6. He, W., Zhong, G., Jiang, N., Wang, B., Fan, X., Chen, C., Chen, X., Huang, J., and Lin, T. (2018). Long noncoding RNA BLACAT2 promotes bladder cancer-associated lymphangiogenesis and lymphatic metastasis. J. Clin. Invest. *128*, 861–875.

7. Chen, L., Zhang, S., Wu, J., Cui, J., Zhong, L., Zeng, L., and Ge, S. (2017). circRNA_100290 plays a role in oral cancer by functioning as a sponge of the miR-29 family. Oncogene *36*, 4551–4561.

8. Chivukula, R.R., Shi, G., Acharya, A., Mills, E.W., Zeitels, L.R., Anandam, J.L., Abdelnaby, A.A., Balch, G.C., Mansour, J.C., Yopp, A.C., et al. (2014). An Essential Mesenchymal Function for miR-143/145 in Intestinal Epithelial Regeneration. Cell *157*, 1104–1116.

9. Janssen, H.L., Reesink, H.W., Lawitz, E.J., Zeuzem, S., Rodriguez-Torres, M., Patel, K., van der Meer, A.J., Patick, A.K., Chen, A., Zhou, Y., et al. (2013). Treatment of HCV infection by targeting microRNA. N. Engl. J. Med. *368*, 1685–1694.

10. Povedano, J.M., Martinez, P., Flores, J.M., Mulero, F., and Blasco, M.A. (2015). Mice with Pulmonary Fibrosis Driven by Telomere Dysfunction. Cell Rep. *12*, 286–299.

11. Fernandez, I.E., and Eickelberg, O. (2012). New cellular and molecular mechanisms of lung injury and fibrosis in idiopathic pulmonary fibrosis. Lancet *380*, 680–688.

12. Booton, R., and Lindsay, M.A. (2014). Emerging role of MicroRNAs and long noncoding RNAs in respiratory disease. Chest *146*, 193–204.

13. Lu, Q., Guo, Z., Xie, W., Jin, W., Zhu, D., Chen, S., and Ren, T. (2018). The lncRNA H19 Mediates Pulmonary Fibrosis by Regulating the miR-196a/COL1A1 Axis. Inflammation *41*, 896–903.

14. Fang, S., Guo, H., Cheng, Y., Zhou, Z., Zhang, W., Han, B., Luo, W., Wang, J., Xie, W., and Chao, J. (2018). circHECTD1 promotes the silica-induced pulmonary endothelial-mesenchymal transition via HECTD1. Cell Death Dis. *9*, 396.

15. Song, X., Cao, G., Jing, L., Lin, S., Wang, X., Zhang, J., Wang, M., Liu, W., and Lv, C. (2014). Analysing the relationship between lncRNA and protein-coding gene and the role of lncRNA as ceRNA in pulmonary fibrosis. J. Cell. Mol. Med. *18*, 991–1003.

16. Liu, H., Wang, B., Zhang, J., Zhang, S., Wang, Y., Zhang, J., Lv, C., and Song, X. (2017). A novel lnc-PCF promotes the proliferation of TGF-β1-activated epithelial cells by targeting miR-344a-5p to regulate map3k11 in pulmonary fibrosis. Cell Death Dis. *8*, e3137.

17. Song, X., Xu, P., Meng, C., Song, C., Blackwell, T.S., Li, R., Li, H., Zhang, J., and Lv, C.J. (2018). lncITPF Promotes Pulmonary Fibrosis by Targeting hnRNP L Depending on Its Host Gene ITGBL1. Mol. Ther. *27*, 380–393.

18. Karreth, F.A., Reschke, M., Ruocco, A., Ng, C., Chapuy, B., Léopold, V., Sjoberg, M., Keane, T.M., Verma, A., Ala, U., et al. (2015). The BRAF pseudogene functions as a competitive endogenous RNA and induces lymphoma in vivo. Cell *161*, 319–332.

19. Liu, B., Li, R., Zhang, J., Meng, C., Zhang, J., Song, X., and Lv, C. (2018). MicroRNA-708-3p as a potential therapeutic target via the ADAM17-GATA/STAT3 axis in idiopathic pulmonary fibrosis. Exp. Mol. Med. *50*, e465.

20. Zhang, J., Liu, H., Song, C., Zhang, J., Wang, Y., Lv, C., and Song, X. (2018). Astilbin ameliorates pulmonary fibrosis via blockade of Hedgehog signaling pathway. Pulm. Pharmacol. Ther. *50*, 19–27.

21. King, T.E., Jr., Pardo, A., and Selman, M. (2011). Idiopathic pulmonary fibrosis. Lancet *378*, 1949–1961.

22. Harrow, J., Frankish, A., Gonzalez, J.M., Tapanari, E., Diekhans, M., Kokocinski, F., Aken, B.L., Barrell, D., Zadissa, A., Searle, S., et al. (2012). GENCODE: the reference human genome annotation for The ENCODE Project. Genome Res. *22*, 1760–1774.

23. ENCODE Project Consortium, Birney, E., Stamatoyannopoulos, J.A., Dutta, A., Guigó, R., Gingeras, T.R., Margulies, E.H., Weng, Z., Snyder, M., Dermitzakis, E.T., Thurman, R.E., et al. (2007). Identification and analysis of functional elements in 1% of the human genome by the ENCODE pilot project. Nature *447*, 799–816.

24. Kumarswamy, R., Bauters, C., Volkmann, I., Maury, F., Fetisch, J., Holzmann, A., Lemesle, G., de Groote, P., Pinet, F., and Thum, T. (2014). Circulating long noncoding RNA, LIPCAR, predicts survival in patients with heart failure. Circ. Res. *114*, 1569–1575.

25. Liu, Y., Ferguson, J.F., Xue, C., Ballantyne, R.L., Silverman, I.M., Gosai, S.J., Serfecz, J., Morley, M.P., Gregory, B.D., Li, M., and Reilly, M.P. (2014). Tissue-specific RNA-Seq in human evoked inflammation identifies blood and adipose LincRNA signatures of cardiometabolic diseases. Arterioscler. Thromb. Vasc. Biol. *34*, 902–912.

26. Poller, W., Tank, J., Skurk, C., and Gast, M. (2013). Cardiovascular RNA interference therapy: the broadening tool and target spectrum. Circ. Res. *113*, 588–602.

27. Li, X., Su, Y., Sun, B., Ji, W., Peng, Z., Xu, Y., Wu, M., and Su, C.; American Association for Cancer Research (2016). An Artificially Designed Interfering lncRNA Expressed by Oncolytic Adenovirus Competitively Consumes OncomiRs to Exert Antitumor Efficacy in Hepatocellular Carcinoma. Mol. Cancer Ther. *15*, 1436–1451.

28. Gong, C., and Maquat, L.E. (2011). lncRNAs transactivate STAU1-mediated mRNA decay by duplexing with 3′ UTRs via Alu elements. Nature *470*, 284–288.

29. Tsai, M.C., Manor, O., Wan, Y., Mosammaparast, N., Wang, J.K., Lan, F., Shi, Y., Segal, E., and Chang, H.Y. (2010). Long noncoding RNA as modular scaffold of histone modification complexes. Science *329*, 689–693.

30. Lee, J.T. (2010). The X as model for RNA's niche in epigenomic regulation. Cold Spring Harb. Perspect. Biol. *2*, a003749.

31. Yap, K.L., Li, S., Muñoz-Cabello, A.M., Raguz, S., Zeng, L., Mujtaba, S., Gil, J., Walsh, M.J., and Zhou, M.M. (2010). Molecular interplay of the noncoding RNA ANRIL and methylated histone H3 lysine 27 by polycomb CBX7 in transcriptional silencing of INK4a. Mol. Cell *38*, 662–674.

32. Kopp, F., and Mendell, J.T. (2018). Functional Classification and Experimental Dissection of Long Noncoding RNAs. Cell *172*, 393–407.

33. Meng, X., Li, X., Zhang, P., Wang, J., Zhou, Y., and Chen, M. (2017). Circular RNA: an emerging key player in RNA world. Brief. Bioinform. *18*, 547–557.

34. Yao, Z., Luo, J., Hu, K., Lin, J., Huang, H., Wang, Q., Zhang, P., Xiong, Z., He, Z., Huang, Z., et al. (2017). ZKSCAN1 gene and its related circular RNA (circZKSCAN1) both inhibit hepatocellular carcinoma cell growth, migration and invasion but through different signaling pathways. Mol. Oncol. *11*, 422–437.

35. Cesana, M., Cacchiarelli, D., Legnini, I., Santini, T., Sthandier, O., Chinappi, M., Tramontano, A., and Bozzoni, I. (2011). A Long Noncoding RNA Controls Muscle Differentiation by Functioning as a Competing Endogenous RNA. Cell *147*, 358–369.

36. Zhang, S., Zhu, D., Li, H., Li, H., Feng, C., and Zhang, W. (2017). Characterization of circRNA-Associated-ceRNA Networks in a Senescence-Accelerated Mouse Prone 8 Brain. Mol. Ther. *25*, 2053–2061.

37. Liang, H., Pan, Z., Zhao, X., Liu, L., Sun, J., Su, X., Xu, C., Zhou, Y., Zhao, D., Xu, B., et al. (2018). LncRNA PFL contributes to cardiac fibrosis by acting as a competing endogenous RNA of let-7d. Theranostics *8*, 1180–1194.

38. Kleaveland, B., Shi, C.Y., Stefano, J., and Bartel, D.P. (2018). A network of noncoding regulatory RNAs acts in the mammalian brain. Cell *174*, 350–362.e17.

39. Keniry, A., Oxley, D., Monnier, P., Kyba, M., Dandolo, L., Smits, G., and Reik, W. (2012). The H19 lincRNA is a developmental reservoir of miR-675 that suppresses growth and Igf1r. Nat. Cell Biol. *14*, 659–665.

40. Yang, Y., Gao, X., Zhang, M., Yan, S., Sun, C., Xiao, F., Huang, N., Yang, X., Zhao, K., Zhou, H., et al. (2018). Novel Role of FBXW7 Circular RNA in Repressing Glioma Tumorigenesis. J. Natl. Cancer Inst. *110*, 1–12.

41. Ruiz-Orera, J., Messeguer, X., Subirana, J.A., and Alba, M.M. (2014). Long non-coding RNAs as a source of new peptides. Elife *3*, e03523.

42. Driskell, J.D., Seto, A.G., Jones, L.P., Jokela, S., Dluhy, R.A., Zhao, Y.P., and Tripp, R.A. (2008). Rapid microRNA (miRNA) detection and classification via surface-enhanced Raman spectroscopy (SERS). Biosens. Bioelectron. *24*, 923–928.